Estimate of the pair correlation functions of nuclei in normal prostate, prostatic intraepithelial neoplasia, and cancer

Luis Santamaría[1], Ildefonso Ingelmo[2], Fernando Teba[3], Rosario Rodríguez[4] and José M. Pozuelo[4]

[1]Department of Anatomy, Histology, and Neuroscience, School of Medicine, Autonomous University of Madrid, Madrid, Spain, [2]Department of Anesthesiology, Hospital Ramón y Cajal, Madrid, Spain, [3]Department of Surgery (Urology), Hospital de La Princesa, School of Medicine, Autonomous University of Madrid, Spain and [4]Department of Medical Basic Sciences, School of Medicine, San Pablo University, CEU, Madrid, Spain

SUMMARY

This study deals with the application of methods of second-order stereology to investigate the spatial distribution of nuclei in normal prostate, prostatic intraepithelial neoplasia and adenocarcinoma. We aimed to identify differences related to the progression of premalignant lesions (PIN) to carcinoma, as well as the spatial changes in relation to tumour grade. Estimation of second-order stereology parameters, such as g(r), (pair correlation function), statistic M, and Clark-Evans aggregation index (CEAI) were employed to investigate the distribution of nuclei.

Linear discriminant analysis (LDA) with M and CEAI as model variables was implemented to classify the cancer cases into two groups according to Gleason score. We found that the point processes of the nuclei in prostatic cancer and normal tissues differed by first-order as well as by second-order properties. In the PIN the mean g-values were intermediate between normal and cancer. The LDA indicates that M and CEAI were able to classify into the correct group of Gleason score more than 90% of the cases analysed. Cancer cases showing a higher degree of disorder in the spatial distribution of nuclei were significantly classified into the group of higher Gleason score. The nuclei in both normal and pathological prostate were not Poisson distributed. Additionally, we found that the progression from normal tissue to carcinoma was accompanied by a progressive increase in spatial disorder which is intermediate in pre-malignant lesions (PIN). The parameters employed were able to classify the cancer cases according to the Gleason score.

Key words: Prostate cancer – PIN – Gleason score – Nuclear patterns – Pair correlation function – Point processes

INTRODUCTION

There are numerous studies on nuclear patterns in prostate carcinoma and prostatic intraepithelial neoplasia (PIN). Most of them make reference to the chromatin distribution and morphometric changes in relation to the process of malignant transformation (Boone et al., 2001; Huisman et al., 2007). Several authors indicate that nuclear texture features allow discrimination of most benign and malignant prostate nuclei (Bartels et al., 1998; Bartels et al., 2001; Huisman et al., 2007; Veltri et al., 2012). For example, some nuclear morphometric score, obtained by automated digital analysis, could be validated for discrimination of benign from cancer nuclei (Gann et al., 2013). Besides, the in-

---

Corresponding author: L. Santamaría. Department of Anatomy, Histology, and Neuroscience. School of Medicine, Autonomous University of Madrid, C/Arzobispo Morcillo 2, 28029-Madrid, Spain. Phone: 34-914975367; Fax: 34-914975353.

E-mail: luis.santamaria@uam.es

clusion of nuclear features in the prognostic factor score may aid in stratifying patients into high-risk and low-risk groups for testing adjuvant therapies for prostate cancer (Partin et al., 1992). Other studies deal with the interrelation of tumour structure and the spatial distribution of prostate cancer nuclei, observing that the Gleason classification matched in part with the classification based on the fractal dimension capacity of the nuclei (Waliszewski et al., 2015).

The distribution of nuclei (either from normal or tumour cells) in a tissue, could be assimilated to the spatial arrangement of a random set of points, and then might be studied by methods related to stochastic geometry (Baddeley et al., 2005). The most basic information is an estimate of the intensity λ of the point process – i.e., the mean number of points (nuclei) per unit reference area. Usually, it is sufficient to estimate λ simply by counting the number of points in the observation windows.

The first-order parameters, as intensity, tell nothing about the geometrical architecture (pattern) of the elements such as blood vessels, glandular acini, or cell nuclei.

To describe arrangements of random sets in space, a well-established approach consists of methods of second-order stereology (Mattfeldt et al., 1993b). Whereas the intensity is a single quantity, the second-order functions provide a series of values as a function of the interpoint distance r. These values indicate which kind of interaction between points or nuclei prevails at a certain distance. This interaction may consist of attraction (clustering) or repulsion, or otherwise there may be no interactive effects between the points at all at a certain distance (Mattfeldt, 2005; Mattfeldt et al., 2006).

Second-order stereology could bring in this respect valuable information about the spatial distribution of nuclei of malignant or premalignant lesions, and probably contribute to an appropriate gradation of tumour aggressiveness. For example, in the case of mammary tumours, the intensity and covariance of the volume fraction of tumour tissue has been analysed by estimation of correlation function k(r), the pair correlation function g(r), and the radial distribution function (RDF r). The clearest distinction between groups was obtained by estimation of g(r) (Mattfeldt et al., 1993a).

The ordinary planar pair correlation function g(r) of the sectional profiles of particles can be used to estimate whether these particles (i.e. nuclei) are showing a tissular distribution with either complete spatial randomness or attraction (clustering), or even repulsion (Mattfeldt, 2005; Mattfeldt et al., 2006). In this sense, the analysis of g(r) has been applied for comparison between normal and tumour blood vessels in the prostate gland (Mattfeldt et al., 2006), and also for the study of distribution of cell nuclei from mammary carcinoma (Mattfeldt, 2011).

The present study deals with the application of methods of second-order stereology to investigate the presence of spatial distribution of nuclei in normal and pathological prostate (prostatic intraepithelial neoplasia and adenocarcinoma). It is intended to identify potential differences in these patterns in relation to the progression of premalignant lesions (PIN) to carcinoma, as well as the spatial changes in relation to tumour grade.

MATERIAL AND METHODS

Material

Fifty four prostate specimens were collected from both La Princesa Hospital (Madrid, Spain), and Madrid Norte-Sanchinarro Hospital (Madrid, Spain): 10 were from adults, (CTR group), age (mean ± SD): 33 ± 8.5; range: 20-47 years. All these specimens were from healthy subjects deceased in traffic accidents, without endocrine or reproductive pathology, and eligible as donors for transplant. The age of the CTR group was under 50 years old to avoid the presence of subclinical hyperplastic changes, relatively frequent above this age (McNeal, 1990). The other 44 were surgical specimens (radical prostatectomy) from patients diagnosed with prostate carcinoma: age (mean ± SD): 70 ± 10, range: 56 to 85 years. In all these cases, the diagnosis of carcinoma was previously confirmed by histopathology. Among these cases, in 18 of them, high-grade PIN lesions (PIN group) were localized and studied. In the remaining 26 tumour cases, the invasive adenocarcinoma was considered (Ca group). All cancer cases were graded according to Gleason score (Epstein et al., 2005) (Table 1) without prior neoadjuvant hormonal therapy. All the ethical requirements were fulfilled in order to obtain the prostatic tissue either at the moment of the multiorganic extraction for transplant (CTR group) or during surgery (PIN and Ca groups). Immediately after extraction, the specimens were fixed during one week in 10% paraformaldehyde in PBS, pH 7.4. After fixation, the specimens from the three groups were thoroughly sectioned into 2-mm-thick slices, performed by isotropic uniform random sampling (IUR sections), in order to preserve the isotropy of the tissue

Table 1. Summary of the Gleason score for the Ca group

Gleason score	percentage of cases
4 (2+2)	4
5 (2+3)	11
6 (3+3)	23
7 (3+4)	62

Summary of the Gleason score for the Ca group. In the column on the left were expressed the total score and the primary and secondary grade (between parenthesis). In the column on the right was expressed the percentage of cases for each score observed, over a total of 26 cases.

(Baddeley et al., 2004).

Tissue processing

All the specimens were processed for paraffin embedding. The paraffin blocks were exhaustively sectioned. Five-µm-thick sections were performed on each block. One from each set of sections was randomly selected and stained by haematoxylin-eosin. All slides were dehydrated in ethanol, and mounted in a synthetic resin (Depex, Serva, Heidelberg, Germany).

Data acquisition

Three fields chosen by systematic random sampling were explored for each section from CTR, PIN and Ca groups. The result was a series of images from the three groups, sized 512 x 680 pixels. The final magnification (x200) was such that 512 pixels represented 327 µm. The images were captured using a colour digital camera DP 70 (Olympus Corporation of the Americas, PA, USA) with a resolution of 12.5 mega-pixels, attached to an Olympus microscope fitted with a motorised stage controlled by the stereological software Cast-Grid (Stereology Software Package, Silkeborg, Denmark). This program controls the XY displacement of the microscope stage and allows the selection of fields to be studied by random systematic sampling after the input of an appropriate sampling fraction (Santamaria *et al.*, 2011).

Subsequently, the images were processed using the public domain Java image processing program, Image J (version 1.48), developed at the US National Institutes of Health and available on the Internet at http://imagej.nih.gov/ij/index.html (Rasband et al., 1995). A binary image was produced where the cell nuclei was shown as black and the reference space (cytoplasm, stroma, etc.) as white.

After digitizing the coordinates of the mass centre of the nuclei profiles on sections (using an appropriate plugin from Image J), exploratory methods of data analysis were applied to characterize the two-dimensional point process of the nuclei. The most basic information is an estimate of the intensity λ of the point process – i.e., the mean number of nuclei per unit reference area (Stoyan et al., 1994). It is important to note that in what follows the term "point" is interchangeable with "nucleus".

Whereas the intensity is a single quantity, second-order functions provide a series of values as a function of the interpoint distance r. For the estimation of these functions, it is advisable to assume stationarity and isotropy in the patterns studied (Mattfeldt, 2005; Mattfeldt et al., 2006).

One of the means of analysing point patterns is the use of statistics based on the co-occurrences of pairs of points. In the present study, the pair correlation function g(r) was employed. The g(r) function is analogous to a probability density function, that is, the derivative of a cumulative distribution function, in our case the K-function (Ripley, 1988; Stoyan et al., 1995), which is a measure of the average number of points found within a set distance r, from each point, divided by the mean intensity (λ) of the pattern. Then, the pair correlation function g(r) may be obtained after differentiation and normalization of K(r) (Mattfeldt, 2005).

As reference model (null hypothesis) for isotropic and stationary point processes, the model of a stationary Poisson point process was used; in this particular case there is no interaction between the points at all distances. The points are distributed independently at random, isotropically and homogeneously in the plane, a state which has been denoted as complete spatial randomness (CSR) of points (Diggle et al., 1991; Diggle, 2003; Schladitz et al., 2003). For a stationary Poisson point process, $g(r) \equiv 1$. In the measured data, values of g(r) below 1 indicate repulsion and values above 1 indicate clustering for point pairs of such a distance r. Hills and valleys above and below the constant value 1 indicate domains of r-values with tendencies of the points for aggregation and repulsion, respectively (Mattfeldt et al., 2006).

Isotropy of nuclei distribution

Prior to estimating the second-order functions is essential to demonstrate the isotropy of the distribution of nuclear population (Mattfeldt et al., 2006). Anisotropy analysis is the study of whether spatial pattern differs along different cardinal axes. For this purpose, the angular correlation between the distribution of the nuclei and certain directions in the plane was estimated. The angular correlation, proposed by Simon G (Simon, 1997), is a method of determining the degree of anisotropy in two-dimensional data. This method calculates the correlation between the distance between pairs points projected onto a vector in a specified direction and the difference in the values associated with those two points.

To run the angular correlation analysis, the data file containing the coordinates of the mass centre of the nuclei profiles were superimposed to a rectangular matrix where each row consists of a specific grid cell: the first column contains the coordinates of the cell, and the subsequent column contains the number of nuclei determined for the cell. The correlation was tested along 360 angular directions. The output of the analysis – i.e., the regression coefficient (R) – was plotted against each angular direction tested (0 to 360 degrees). The analysis was performed in all the groups studied, using the software for spatial statistics, PASSAGE (Version 2.0) (Rosenberg et al., 2011).

Calculation of the pair correlation function

The g(r) function was calculated by all the sets of nuclear profiles obtained in the three groups of study using the Spatstat, which is a package for the statistical analysis of spatial data. Currently, it

deals mainly with the analysis of patterns of points in the plane, and runs in R (version 2.15.1), which is a language and environment for statistical computing and graphics (Baddeley et al., 2005).

In order to test whether the planar point patterns provided for the distribution of cell nuclei for the groups of study differ from a CSR distribution of points, envelopes for the g(r) function were done for each of the images analysed.

The "envelope" command from Spatstat performs simulations and computes envelopes of a summary statistic based on the simulations. These envelopes can be used to assess the goodness-of-fit of a point process model to point pattern data (Diggle, 2003).

Briefly, to test CSR for a point pattern (i.e. a nuclei pattern from a case) we generate 99 simulations of CSR (i.e. 99 simulated point patterns each being a realisation of the uniform Poisson point process) with the same intensity as the given pattern. The simultaneous critical envelopes obtained allow us to perform a Monte Carlo test (Ripley, 1981). The test rejects the null hypothesis if the graph of the observed function lies outside the envelope at any value of r.

In each group of study, the values of g(r) were calculated pointwise (i.e. for each value of the distance r), and their confidence intervals (at 95%) obtained. These values, together with their simulated envelopes were plotted as function of the interpoint distance (r).

Simultaneously, the intensity (λ) of the process, expressed as the average number of nuclei per square micron of the reference space ± CI (confidence intervals at 95%), was also estimated for each group of study.

To test for statistical differences between the mean of g-functions at fixed r-values, bootstrap tests were performed (Mattfeldt et al., 2006). These methods were used to compute confidence intervals for the comparison of g(r) functions among the three groups of study. Bootstrap methods are defined as computer-intensive methods based on independent resampling of an empirical data set with replacement (Mattfeldt, 2011). The bootstrap method was developed by Bradley Efron in 1979 (Efron et al., 1993) and consists basically of an independent random resampling of the sample data with replacement. It is a computer-based method largely free of statistical model assumptions. In the present study, the bootstrap statistic g(r) was computed from 1000 bootstrap samples. It is assumed that the distribution of the bootstrap statistics approximates the distribution of the statistic in the population (Mattfeldt et al., 2006).

The confidence intervals (at 95%) obtained r-wise by bootstrapping, together with the mean values for each r of the g-functions from CTR, PIN, and Ca groups were plotted.

Evaluation of individual g-functions

In addition to the local computation of confidence intervals for fixed r, each estimated g(r) function per visual field was evaluated with a method presented by Stoyan et al. 1990 (Stoyan et al., 1990) and Stoyan et al. 1994 (Stoyan et al., 1994). This procedure estimates a statistic (M) using the next formula:

Where:

$$M = \frac{g_{max} - g_{min}}{r_{min} - r_{max}}$$

g_{max}: First maximum of the g(r) function g_{min}: The following minimum to g_{max} r_{max}: The r-value corresponding to g_{min}

The statistic M is related to the global degree of disorder in the spatial point pattern (Mattfeldt et al., 2006). Large values indicate a high degree of order and may be used as a tool to summarize the course of the g-function by a single quantity. The M values were calculated for CTR, PIN, and Ca groups, and expressed as mean ± CI (confidence intervals at 95%)
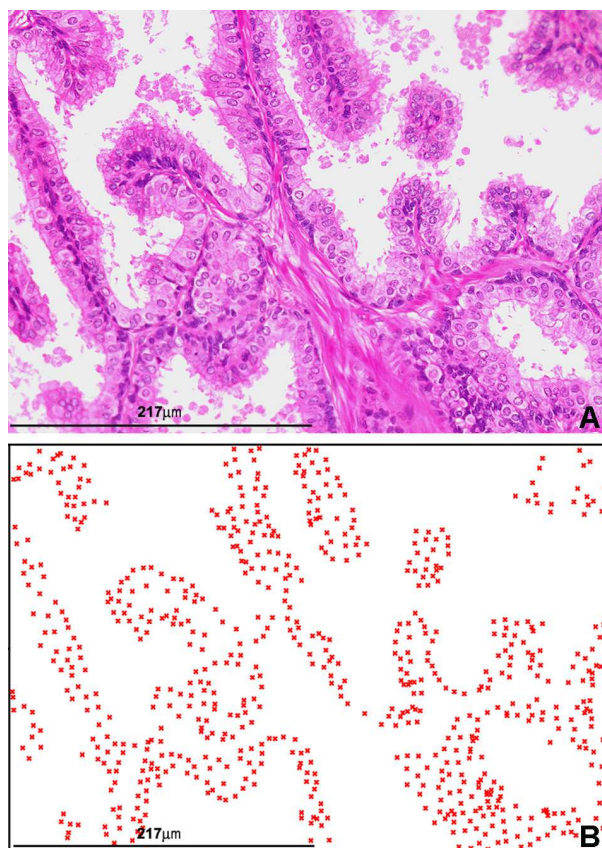

Fig. 1. In **(A)**, prostate acini from the peripheral zone of normal prostate from CTR group can be seen. Haematoxylin-eosine. In **(B)**, the center masses of the nuclei from (A) are depicted; well ordered layers of points showing a clustered pattern could be seen. Scale bar, 127 μm.

Estimation of Clark-Evans Aggregation Index

The Clark-Evans aggregation index (CEAI) is a crude measure of clustering or ordering of a point pattern. It is the ratio of the observed mean nearest neighbour distance in the pattern to that expected for a Poisson point process of the same intensity. A value CEAI > 1 suggests repulsion while CEAI < 1 suggests clustering (Clark et al., 1954).

Without correction for edge effects, the value of CEAI will be positively biased. Edge effects arise because, for a point close to the edge of the window, the true nearest neighbour may actually lie outside the window. Hence observed nearest neighbour distances tend to be larger than the true nearest neighbour distances. The theoretical expected value of mean nearest neighbour distance under a Poisson process was adjusted for edge effects by the edge correction of Donnelly (Donnelly, 1978). To calculate CEAI was used the command "clarkevans" from Spatstat Package (Baddeley et al., 2005). This command performs a hypothesis test of clustering or ordering of the point pattern. The null hypothesis is Complete Spatial Randomness, i.e. a uniform Poisson process. The alternative (two-sided) hypothesis is that CEAI ≠ 1 corresponding to a clustered or regular pattern. The estimate was performed for CTR, PIN, and Ca groups, and expressed as mean ± CI (confidence intervals at 95%).

Statistical comparisons

The differences among the parameters measured (λ, M, and CEAI) for CTR, PIN, and Ca groups were compared by ANOVA, comparisons between the means for all the groups studied were performed by the Newman–Keuls test ($p < 0.05$).

Discriminant analysis to classify cancer cases after Gleason score

The Gleason scoring was organized in two groups defined by a cut-off point located at the 50th percentile, namely: Gleason < 7 and, Gleason ≥ 7. In order to determine the variables that most accurately classify cancer cases in the two groups defined by Gleason grading, stepwise linear discriminant analysis (LDA) (Huisman et al., 2007) was applied to the Ca group for the set of variables estimated: λ, M, and CEAI. Discriminant variables were selected according to Wilks' lambda: at each step, the variable that minimises the overall Wilks' lambda or maximises the associated F statistic is selected (F to enter = 3.84 and F to
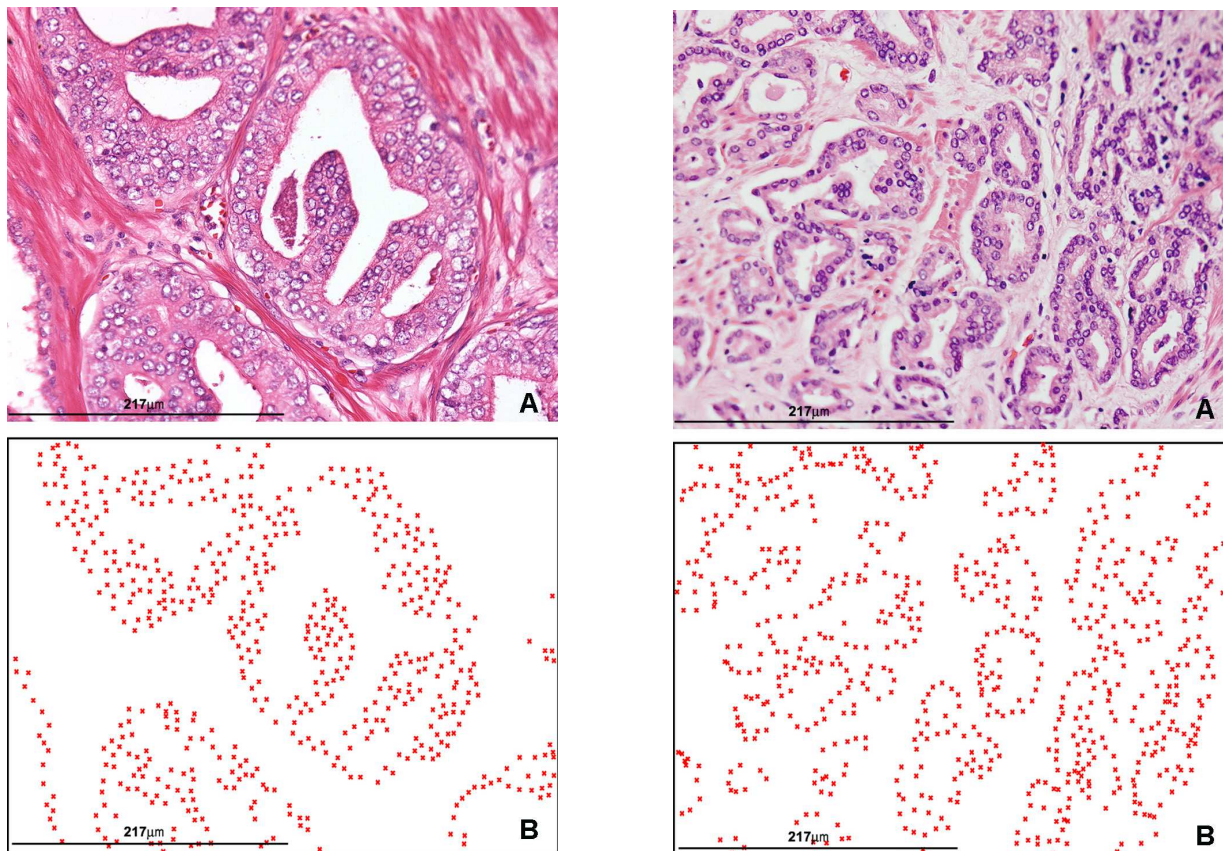

Fig. 2 (left). (A) Three acini with prostate intraepithelial neoplasia from PIN group can be seen. Haematoxylin-eosine. **(B)** The center masses of the nuclei from (A) are depicted; points showing a clustered pattern were displayed. Scale bar, 127 μm.

Fig. 3 (right). (A) Tumour acini with a Gleason 3 score from Ca group are illustrated Haematoxylin-eosine. **(B)** The centre masses of the nuclei from (A) are depicted, with points showing a pattern with moderate dispersion. Scale bar,

remove = 2.71). Wilks' lambda statistic explains the rate of total variability that is not due to differences among groups. A lambda of 1 means that the mean of the discriminant scores is the same in all groups and there is no variability between groups, while a lambda near 0 means that there is a significant difference among groups. Therefore, Wilks' lambda provides a test of the null hypothesis that the population means are equal. The larger lambda in the less discriminating power is present (Hair et al., 1998).

The estimates of discriminant variables selected, expressed as mean ± CI, were compared between the two groups of Gleason (<7 and ≥ 7) by a Student t test (p<0.05).

RESULTS

Descriptive findings

From a descriptive point of view, no relevant differences have been detected in the distribution of the centres of mass of prostatic epithelial nuclei,
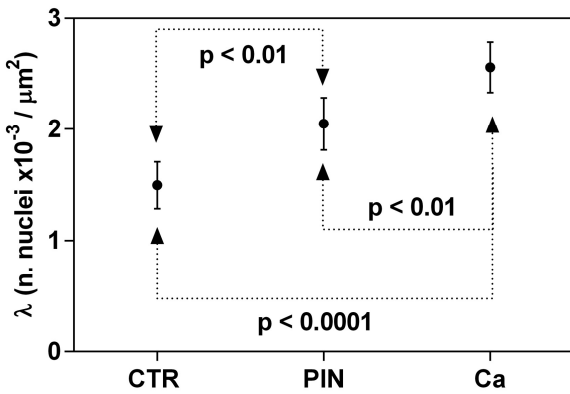
Fig. 4 (above) Graph indicating the intensity of the process of points (number of nuclei x 10^{-3} / μm^2) for normal prostate (CTR), PIN group (PIN) and cancer group (Ca). All the values are expressed as mean ± CI (95%). The values with significant differences (p<0.05) between them are connected by zigzag lines with arrowheads in both endings.
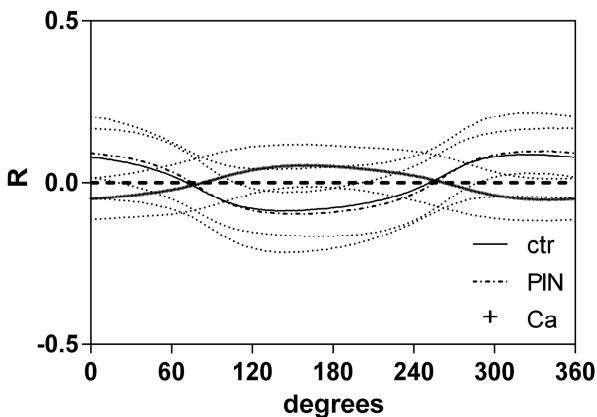
Fig. 5. Graph indicating the regression coefficient (R) plotted against the angular directions tested (0 to 360 degrees). The confidence intervals for the R values (dotted lines) from CTR, PIN and Ca cases show a wide overlapping.
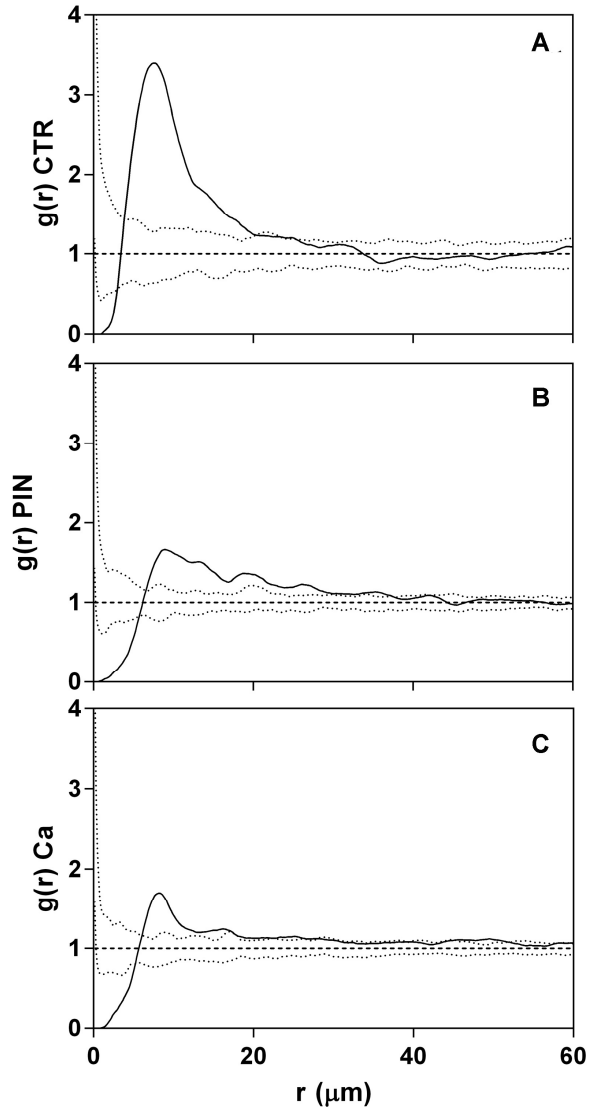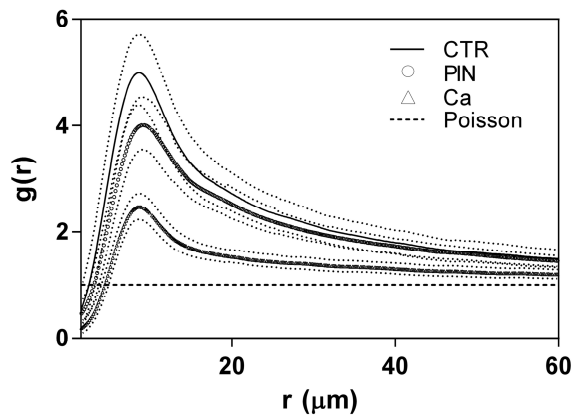
Fig. 6 (above). (A) Estimated g(r) from a selected visual field of tumour-free prostatic tissue (CTR group). Note the hard-core effect in the beginning, then weaker repulsion, and thereafter first maximum and first minimum. **(B)** Estimated g(r) from a selected visual field of PIN lesion (PIN group). The extension of hard-core effect is similar to that observed in (A). Here the curve ascends less steeply. **(C)** Estimated g(r) from a selected visual field of prostatic cancer tissue (Ca group). The extension of hard-core effect is similar to that observed in (A) and (B). Here the curve ascends less steeply than in CTR group. In all the cases the first maximum of g(r) is located over the CSR simulated envelope (dotted lines). The straight line in g(r) ≡ 1 in the three images represents the graph of a Poisson process. In the X axis, the interpoint distance (r) was

when images from normal prostate, PIN, and carcinoma were compared (Figs. 1-3).

Nevertheless, the relative amount per unit of area (intensity of point process) of the nuclei was significantly increased in Ca group and PIN groups in comparison with CTR group, (Fig. 4).

Isotropy of nuclei distribution

The estimates of the angular correlation did not

Fig. 7. Mean values and 95% confidence intervals for the g(r) functions of the nuclei for tumour-free tissue (solid line), PIN lesions (empty circles), and cancer tissue (empty triangles). The confidence intervals (CI) were obtained r-wise by bootstrapping. The CI of the g(r) functions of CTR and PIN groups are widely overlapped for all the r- domains. The CI of g(r) function for Ca group lies below those from CTR and PIN groups in

and attaining thereafter positive values, usually quickly mounting to a first maximum g_{max} and then descending to a first minimum g_{min}. In PIN and Ca cases the curve ascends less steeply than in CTR specimens. In all the cases the first maximum of g(r) is widely located over the simulated envelope for CSR process; the length of r where g(r) = 0, is similar for all the three groups of cases (Fig. 6 A-C).

Estimates of the mean g-functions per group were obtained and 95% confidence intervals (CI) were computed by bootstrap methods. Results are shown in Fig.7. The profile of the g(r) function for Ca group lies outside and below of the CI of g(r) from CTR and PIN groups. Although the g(r) of PIN group falls below the CTR group, their CI extensively overlap (Fig. 7).
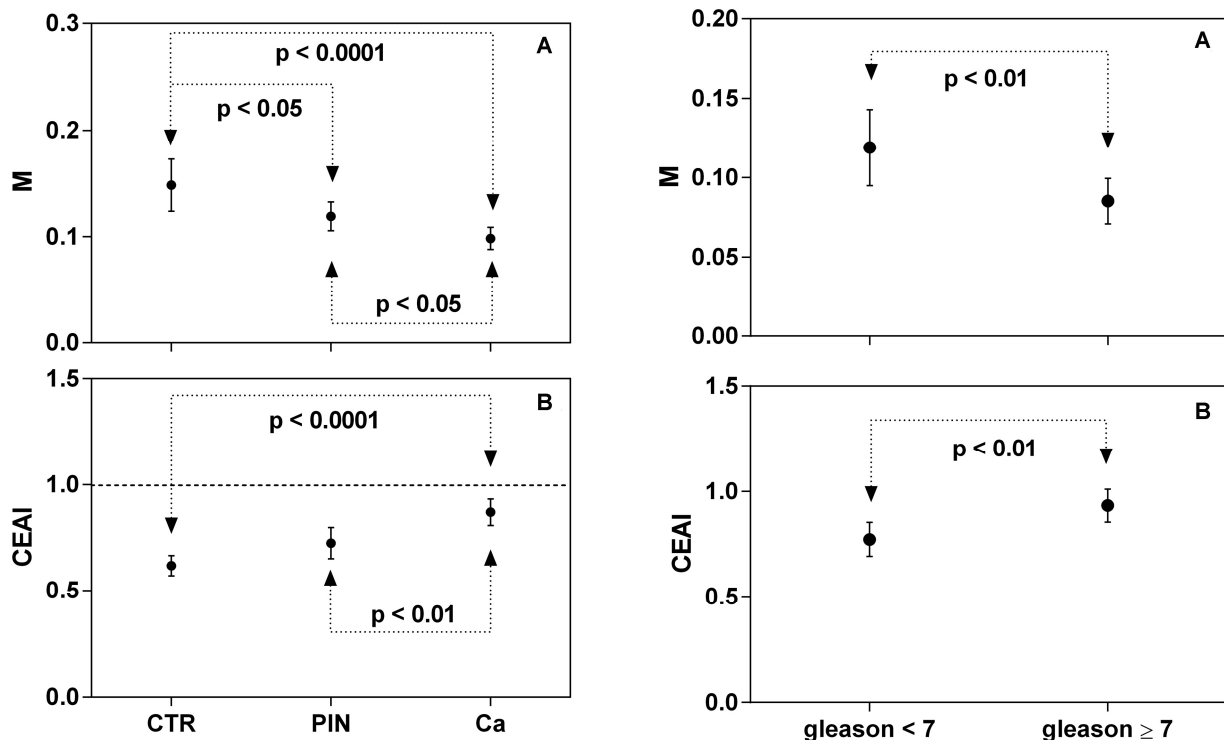
show significant correlation between the λ of point data (intensity of the nuclei) with the angular directions explored for all the groups of the study (Fig. 5).

Calculation of the pair correlation function

In all the groups studied, the g(r) functions lie outside of the simulated CSR envelopes for a wide range of the interpoint distance (r) (Fig. 6 A-C).

For all the cases, the curves began with a flat curve segment where g(r) = 0 (hard- core effect)

Fig. 8 (left). Graph indicating **(A)** the statistic M, and **(B)** the Clark- Evans aggregation index (CEAI) for normal prostate (CTR), PIN group (PIN) and cancer group (Ca). All the values are expressed as mean ± CI (95%). The values with significant differences (p<0.05) between them are connected by zigzag lines with arrowheads in both endings. The dashed line for CEAI ≡ 1 (B) indicates the CEAI of points with CSR distribution.

Fig. 9 (right). Graph indicating **(A)** the statistic M, and **(B)** the Clark- Evans aggregation index for cancer cases classified according to the Gleason score (Gleason < 7, Gleason ≥ 7). The values are expressed as mean ± CI (95%). The differences between the two groups were significant (p<0.01) in (A) and (B).

The statistic M showed a progressive decrease from CTR to Ca groups, showing an intermediate value in the PIN group (Fig. 8 A). In all the cases the differences were significant. The Clark Evans aggregation index showed an opposite behaviour to M: The larger value was in CTR group, the lowest was observed in Ca group, while in PIN group showed an intermediate value (Fig. 8 B). In all the cases the differences were also significant.

Discriminant analysis

The discriminant analysis for Gleason groups reveals that the intensity of process (λ) was excluded from analysis, because the F to enter was below the minimum value (3.84). The two remaining variables in order of classificatory power were: M and CEAI. With these two variables in the model, 92% of the cancer cases were correctly classified into the Gleason groups. Table 2 shows the significant reduction of the Wilks' lambda statistics with these variables included in the model. The estimates of mean values ± CI of these variables for each Gleason groups are displayed in Fig.9.

DISCUSSION

Compared with normal prostatic tissue, the intensity of the point process, i.e. number of nuclear profiles per square micron of tissue, is significantly increased in PIN and prostatic cancer.

As was expected, the measurements of angular correlation indicate that the intensity of process shows no preferred direction. Therefore isotropy condition is met, which is the indispensable requirement for an unbiased estimation of g(r) (Mattfeldt, 2005; Mattfeldt et al., 2006).

Using bootstrap inference methods for r-wise comparisons of mean g-values, a significant decrease of the mean g-values at various distances could be demonstrated in the prostatic cancer group. Hence, the point processes of the nuclei in prostatic cancer tissue and normal prostatic tissue differ by first-order as well as by second-order properties. However, in the PIN group the mean g-values were similar to the observed for CTR cases, and intermediate between normal and cancer.

Parallel to these changes, it could be shown that the height of the first maximum of the pair correlation function declined in the carcinoma group.

On the other hand, the graph of the g(r) function

for all the three groups lies outside the simulated CSR envelope at any value of r. Therefore, the null hypothesis that identifies the distribution of nuclei studied with a Poisson process can be rejected.

In all the groups, an initial short segment of r-values where g(r) = 0 was observed. This is a hard-core effect, because for the cell nuclei no overlapping is possible. This hard-core effect was roughly similar in the three groups. Then, the increase of the intensity λ of nuclei in the cancer group was not accompanied by a diminished hard-core distance in the cancerous group, which might have been expected. It cannot be excluded that the g(r) changes are partially due to a higher intensity of the nuclei in the PIN and carcinoma groups (Mattfeldt et al., 2006).

Another explanation for the observed alterations of the g(r)-function is a true change of the inner order of the neoplastic tissue as compared with the normal tissue that affects the nuclei arrangement, irrespective of the intensity of the process. In this sense, the distribution of nuclei from PIN lesions shows a larger similarity with those of controls. These changes on nuclear arrangement in neoplastic condition have been also described by other authors using fractal measurements, indicating that the spatial distribution of cancer cell nuclei changes during tumour progression (Waliszewski et al., 2015).

The evolution of statistic M indicates a progressive increase of disorder in the distribution of nuclei from normal to carcinoma cases, the results being from PIN intermediate. As expected, this was opposite to the detected for Clark Evans aggregation index, with a greater clustering in the nuclei from control prostates (arranged in normal acini) than in cancer cases (more dispersed in tumour nests). These results were in agreement to those described in other tumour conditions as breast cancer, where the estimation of g(r) showed that short-range, tubular pattern as well as long-range, lobular architecture are better preserved in benign than in malignant lesions (Mattfeldt et al., 1993a).

It is interesting to note that PIN cases show, for almost all the parameters analysed, an intermediate position between normal and cancer prostate, but, frequently the PIN values of the measurements estimated do not show significant differences with those of the controls. There is evidence that many prostate cancers are preceded by or accompanied with a pre-malignant change in the epithelial cells, known as prostatic intraepithelial neoplasia (PIN) (Sequeiros et al., 2015). The findings described in the present study support the progression of the neoplastic transformation from normal nuclei to PIN pre-neoplastic nuclei and, subsequently, to tumour nuclei (Bartels et al., 1998).

Table 2. Discriminant analysis to classify the cancer cases after Gleason score.

Entered variable[1]	Wilks´ lambda[2]	F[3]	p[4]
CEAI	0.733	8.732	0.007
M	0.535	10.008	0.001

[1]Selected variables. [2]This column shows the Wilks' lambda for every variable entered. [3]F distribution of Snedecor, the F minimum value for entering the variables was 3.84. [4]Level of significance p < 0.05.

Different histological grading systems have been developed including the most frequently used Gleason system (Epstein, 2010; Gleason, 1977). The Gleason score, is a measure of heterogeneity, that is, non-uniformity in structural composition of cancer tissue (Waliszewski et al., 2015). This structural disorder might affect the patterns of spatial distribution of nuclei, then the Gleason scoring can be put in relation to parameters of second-order stereology investigated in the present study.

The results of LDA indicate that when M and CEAI variables are introduced in the model, they were able to classify in the correct group of Gleason score more of the 90% of the cases analysed. Besides, cancer cases showing a higher degree of disorder in the spatial distribution of nuclei (low M, high CEAI) were significantly classified into the group of higher Gleason score. These findings agree with those observed by other authors, indicating that the partial loss of epithelial interaction as evidenced by changes in the g(r) is more pronounced in the more malignant lesions (Mattfeldt et al., 1993b).

Summarizing, the next conclusions can be drawn:

The application of second-order stereology tools as g(r) function and aggregation indices provides valuable information about the spatial distribution of nuclei in normal and pathologic prostate, indicating: a) In normal, pre-neoplastic, and neoplastic prostate acini, the distribution of nuclei was arranged in a pattern that cannot be assimilated to a Poisson distribution – i.e., different from a structure with complete spatial randomness; b) the progression from normal tissue to prostate carcinoma is accompanied by a progressive decrease of nuclear clustering (i.e., an increase of spatial disorder), which is intermediate in premalignant lesions as PIN.

The second-order statistic tools were able to classify the cancer cases according to the Gleason score, showing a high Gleason grade those cases with more degree of disorder in the spatial distribution of nuclei.

REFERENCES

BADDELEY A, TURNER R (2005) Spatstat: An R package for analyzing spatial point patterns. *J Statist Software*, 12: 1-42.

BADDELEY A, VEDEL JENSEN EB (2004) *Stereology for Statisticians*. Chapman & Hall/CRC Press; Boca Ratón, Florida, United States.

BARTELS PH, DA SILVA VD, MONTIRONI R, HAMILTON PW, THOMPSON D, VAUGHT L, BARTELS HG (1998) Chromatin texture signatures in nuclei from prostate lesions. *Anal Quant Cytol Histol*, 20: 407-416.

BARTELS PH, MONTIRONI RM, BOSTWICK D, MAR-

SHALL J, THOMPSON D, BARTELS HG, KELLEY D (2001) Karyometry of secretory cell nuclei in high-grade PIN lesions. *Prostate*, 48: 144-155.

BOONE CW, LIEBERMAN R, MAIRINGER T, PALCIC B, BACUS J, BARTELS P (2001) Computer-assisted image analysis-derived intermediate endpoints. *Urology*, 57: 129-131.

CLARK PJ, EVANS FC (1954) Distance to nearest neighbour as a measure of spatial relationships in populations. *Ecology*, 35: 445-453.

DIGGLE PJ (2003) *Statistical Analysis of Spatial Point Patterns*. 2nd ed. Arnold, USA.

DIGGLE PJ, LANGE N, BENES FM (1991) Analysis of variance for replicated spatial point patterns in clinical neuroanatomy. *J Am Statist Ass*, 86: 618-625.

DONNELLY KP (1978) Simulations to determine the variance and edge effect of total nearest-neighbour distance. In: Hodder I, (ed). *Simulation methods in archaeology*. Cambridge University Press, Cambridge, London, pp 91-95.

EFRON B, TIBSHIRANI RJ (1993) *An Introduction to the Bootstrap*. Chapman & Hall, New York.

EPSTEIN JI (2010) An update of the Gleason grading system. *J Urol*, 183: 433-440.

EPSTEIN JI, ALLSBROOK WC, JR, AMIN MB, EGEVAD LL (2005) The 2005 International Society of Urological Pathology (ISUP) Consensus Conference on Gleason Grading of Prostatic Carcinoma. *Am J Surg Pathol*, 29: 1228-1242.

GANN PH, DEATON R, AMATYA A, MOHNANI M, RUETER EE, YANG Y, ANANTHANARAYANAN V (2013) Development of a nuclear morphometric signature for prostate cancer risk in negative biopsies. *PLoS One*, 8: e69457.

GLEASON DF (1977) Histologic grading and clinical staging of prostatic carcinoma. In: Tannenbaum M (ed). *Urologic Pathology*. Lea and Febiger, Philadelphia, pp 171-198.

HAIR JF, ANDERSON RE, TATHAM RL, BLACK WC (1998) *Multivariate data analysis*. 5th ed. Prentice Hall, Upper Saddle River, New Jersey (USA).

HUISMAN A, PLOEGER LS, DULLENS HF, JONGES TN, BELIEN JA, MEIJER GA, POULIN N, GRIZZLE WE, VAN DIEST PJ (2007) Discrimination between benign and malignant prostate tissue using chromatin texture analysis in 3-D by confocal laser scanning microscopy. *Prostate*, 67: 248-254.

MATTFELDT T (2005) Explorative statistical analysis of planar point processes in microscopy. *J Microsc*, 220: 131-139.

MATTFELDT T (2011) A brief introduction to computer-intensive methods, with a view towards applications in spatial statistics and stereology. *J Microsc*, 242: 1-9.

MATTFELDT T, ECKEL S, FLEISCHER F, SCHMIDT V (2006) Statistical analysis of reduced pair correlation functions of capillaries in the prostate gland. *J Microsc*, 223: 107-119.

MATTFELDT T, FREY H, ROSE C (1993a) Second-

order stereology of benign and malignant alterations of the human mammary gland. *J Microsc*, 171: 143-151.

MATTFELDT T, VOGEL U, GOTTFRIED HW, FREY H (1993b) Second-order stereology of prostatic adeno-carcinoma and normal prostatic tissue. *Acta Stereol*, 12: 203-208.

MCNEAL J (1990) Pathology of benign prostatic hy-perplasia. Insight into etiology. *Urol Clin North Am*, 17: 477-486.

PARTIN AW, STEINBERG GD, PITCOCK RV, WU L, PIANTADOSI S, COFFEY DS, EPSTEIN JI (1992) Use of nuclear morphometry, gleason histologic scor-ing, clinical stage, and age to predict disease-free survival among patients with prostate cancer. *Cancer*, 70: 161-168.

RASBAND WS, BRIGHT DS (1995) NIH image: A pub-lic domain image processing program for the Macin-tosh. *Microbeam Anal Soc J*, 4: 137-149.

RIPLEY BD (1981) *Spatial statistics*. John Wiley & Sons, Hoboken, Nueva Jersey, USA.

RIPLEY BD (1988) *Statistical Inference for Spatial Pro-cesses*. Cambridge University Press, Cambridge.

ROSENBERG MS, ANDERSON CD (2011) PAS-SaGE: Pattern Analysis, Spatial Statistics and Geo-graphic Exegesis. Version 2. *Methods in Ecology and Evolution*, 2: 229-232.

SANTAMARIA L, INGELMO I, RUIZ J, TEBA F (2011) Study of the distribution of microvessels in normal and pathologic prostate using an information-based similarity analysis. *J Microsc*, 243: 303-314.

SCHLADITZ K, SARKKA A, PAVENSTADT I, HAF-ERKAMP O, MATTFELDT T (2003) Statistical analy-sis of intramembranous particles using freeze frac-ture specimens. *J Microsc*, 211: 137-153.

SEQUEIROS T, BASTAROS JM, SANCHEZ M, RIGAU M, MONTES M, PLACER J, PLANAS J, DE TORRES I, REVENTÓS J, PEGTEL DM, DOLL A, MOROTE J, OLIVAN M (2015) Urinary biomarkers for the detection of prostate cancer in patients with high-grade prostatic intraepithelial neoplasia. *Prostate*, 75: 1102-1113.

SIMON G (1997) An angular version of spatial correla-tions, with exact significance tests. *Geographical Analysis*, 29: 267-278.

STOYAN D, KENDALL WS, MECKE J (1995) *Stochas-tic Geometry and its Applications*. 2nd ed. Wiley, Chichester, West Sussex, United Kingdom.

STOYAN D, SCHNABEL HD (1990) Description of relations between spatial variability of microstructure and mechanical strength of alumina ceramics. *Ceram Intern*, 19: 11-18.

STOYAN D, STOYAN H (1994) *Fractals, Random Shapes and Point Fields. Methods of Geometrical Statistics*. Wiley, Chichester, West Sussex, United Kingdom.

VELTRI RW, CHRISTUDASS CS, ISHARWAL S (2012) Nuclear morphometry, nucleomics and pros-tate cancer progression. *Asian J Androl*, 14: 375-384.

WALISZEWSKI P, WAGENLEHNER F, GATTENLOH-NER S, WEIDNER W (2015) On the relationship between tumour structure and complexity of the spa-tial distribution of cancer cell nuclei: a fractal geomet-rical model of prostate carcinoma. *Prostate*, 75: 399-414.